JCTC Journal of Chemical Theory and Computation

pH Dependence of a 3_{10}-Helix versus a Turn in the M-Loop Region of PDE4: Observations on PDB Entries and an Electronic Structure Study

Dandamudi Usharani,[†,‡] Palakuri Srivani,[§] G. Narahari Sastry,[§] and Eluvathingal D. Jemmis*[,‡]

School of Chemistry, University of Hyderabad, Hyderabad 500046 India, Department of Inorganic and Physical Chemistry, Indian Institute of Science, Bangalore 560012, India, and Molecular Modeling Group, Organic Chemical Sciences, Indian Institute of Chemical Technology, Tarnaka, Hyderabad 500007, India

Received October 6, 2007

Abstract: Available X-ray crystal structures of phosphodiesterase 4 (PDE 4) are classified into two groups based on a secondary structure difference of a 3_{10}-helix versus a turn in the M-loop region. The only variable that was discernible between these two sets is the pH at the crystallization conditions. Assuming that at lower pH there is a possibility of protonation, thermodynamics of protonation and deprotonation of the aspartic acid, cysteine side chains, and amide bonds are calculated. The models in the gas phase and in the explicit solvent using the ONIOM method are calculated at the B3LYP/6−31+G* and B3LYP/6−31+G*:UFF levels of theory, respectively. The molecular dynamics (MD) simulations are also performed on the M-loop region of a 3_{10}-helix and a turn with explicit water for 10 ns under NPT conditions. The isodesmic equations of the various protonation states show that the turn containing structure is thermodynamically more stable when proline or cysteine is protonated. The preference for the turn structure on protonation (pH = 6.5−7.5) is due to an increase in the number of the hydrogen bonding and electrostatic interactions gained by the surrounding environment such as adjacent residues and solvent molecules.

Introduction

Phosphodiesterases (PDE) are metalloenzymes which hydrolyze the phosphodiesterase bond of cyclic adenosine 3′,5′-monophosphate (cAMP) and guanosine 3′,5′-monophosphate (cGMP) into the corresponding 5′-nucleotides (AMP and GMP) in various cells.[1a,b] The second messenger (cAMP and cGMP) concentration affects the specific protein phosphorylation cascades. Hence, these isozymes play a vital role in the regulation of various physiological functions like visual response, smooth muscle relaxation, platelet aggregation, immune response, cardiac contractibility, etc. They are the therapeutic targets for cardiovascular, inflammatory, and erectile dysfunction diseases.[1c,d] Among the 12 PDE isozymes, PDE4 and PDE5 have received much attention in the recent years.[1–3] The PDE4 catalyze specifically cAMP (Scheme 1A). The abundance of PDE4 in various inflammatory cells such as eosinophils, T cells, B cells, and neutrophils made it a keen target for the inflammatory diseases such as asthma, chronic obstructive pulmonary disease (COPD), allergic rhinitis, type II diabetics, and rheumatoid arthritis.[2b,c]

There are various classes of novel orally active PDE4 inhibitors discovered in this decade. Based on the structural motifs, PDE4 inhibitors can be broadly classified into three categories as xanthines, catechol ethers, and hetrocyclics (nitraquanzone, benzofurans, indoles, isoquinoline, pyridopyrimidinones, pyrazolepyridines, etc). Rolipram that belongs to catechol ether type has been reported as the first selective PDE4 inhibitor (Scheme 1A). The first-generation PDE4 inhibitors rolipram, RO-20-1724 (mesopram), and

* Corresponding author e-mail: jemmis@ipc.iisc.ernet.in.
[†] University of Hyderabad.
[‡] Indian Institute of Science.
[§] Indian Institute of Chemical Technology.

10.1021/ct700261b CCC: $40.75
Published on Web 05/15/2008

Scheme 1. A) Structures of Substrate cAMP and Inhibitor Rolipram of the PDE4, B) Secondary Structure of PDE4 in the M-Loop Region Existing as a 3_{10}-Helix (Red Color) and a Turn (Green Color),[a] and C) Schematic 2-D Representation of the 3_{10}-Helix Conformation[b,c]

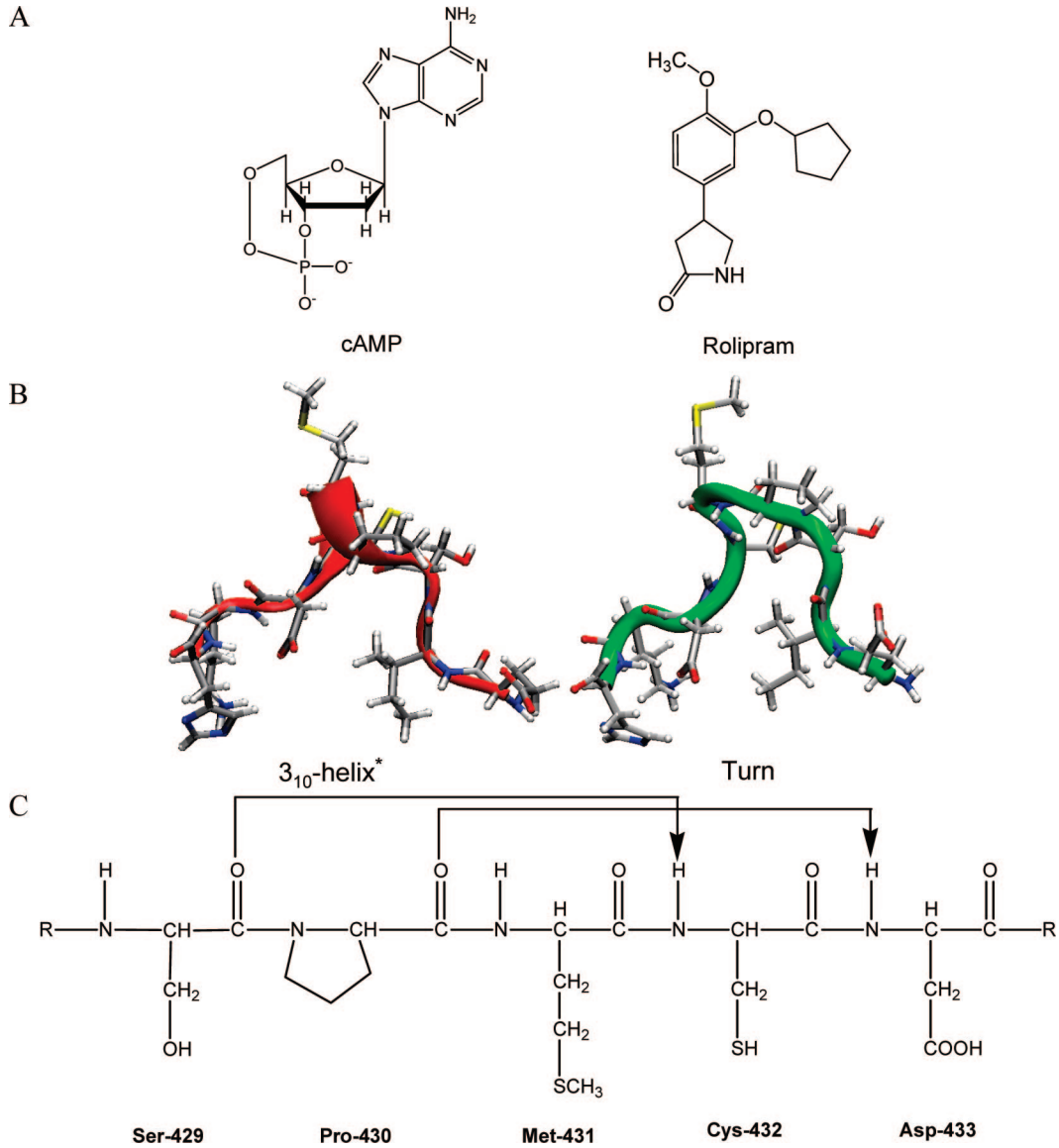

[a] These are shown along with the amino acids represented as a capped stick model. [b] The hydrogen bonds are shown as lines and residue numbering is given for PDE4B. [c] The 3_{10}-helix is formed when the N−H group of an amino acid forms a hydrogen bond with the C=O group of the amino acid three residues earlier ($i+3 \rightarrow i$ hydrogen bonding).[13]

zardaverine are discarded from clinical trials due to the side effects like nausea, vomiting, dyspepsia, headache, and emesis.[2d] The second-generation rolipram analogs (cilomilast, roflumilast, and most potent piclamilast) that are now in clinical trials are also suffering from low therapeutic ratio.[2e] Among the various strategies for overcoming the side effects, subtype selectivity of PDE4 is a focus of investigation.[1,2]

Lack of the 3-dimensional structure of a target protein is usually a bottleneck for rational drug design. In the last couple of years there has been a dramatic increase in the number of crystal structures of PDE4 class of enzymes in the protein data bank (PDB). Despite the availability of 39 X-ray structures along with cocrystals for PDE4, progress toward drugs without undesired side effects has been marginal. Our interest in the modeling of the subtype selective PDE4 drug candidates brought us to a close examination of these crystal structures. We found that there is a characteristic secondary structural conformation difference in the PDE4 crystal structures.[4–10] Out of the 35 PDE4B and 4D crystal structures 12 of them have a 3_{10}-helix and the rest have a turn in the M-loop region[6b] which is near to the active site pocket. The four crystal structures, one for each of the PDE4 subtypes are yet to be deposited.[11] The distinct pattern of a secondary structure in the highly flexible M-loop region is prominent in these crystal structures (Scheme 1B). According to the standard protein structural rules, three and a half residues are required per turn of an α-helix. The hydrogen of the amide group of the first residue forms a hydrogen bond with the oxygen of the amino-terminal peptide bond of the fourth residue in an α-helix, whereas in a 3_{10}-helix it forms with the third residue.[12,13] Here we would like to know the factor responsible for this secondary structural change in the M-loop region. The methionine of the M-loop region has a hydrophobic interac-

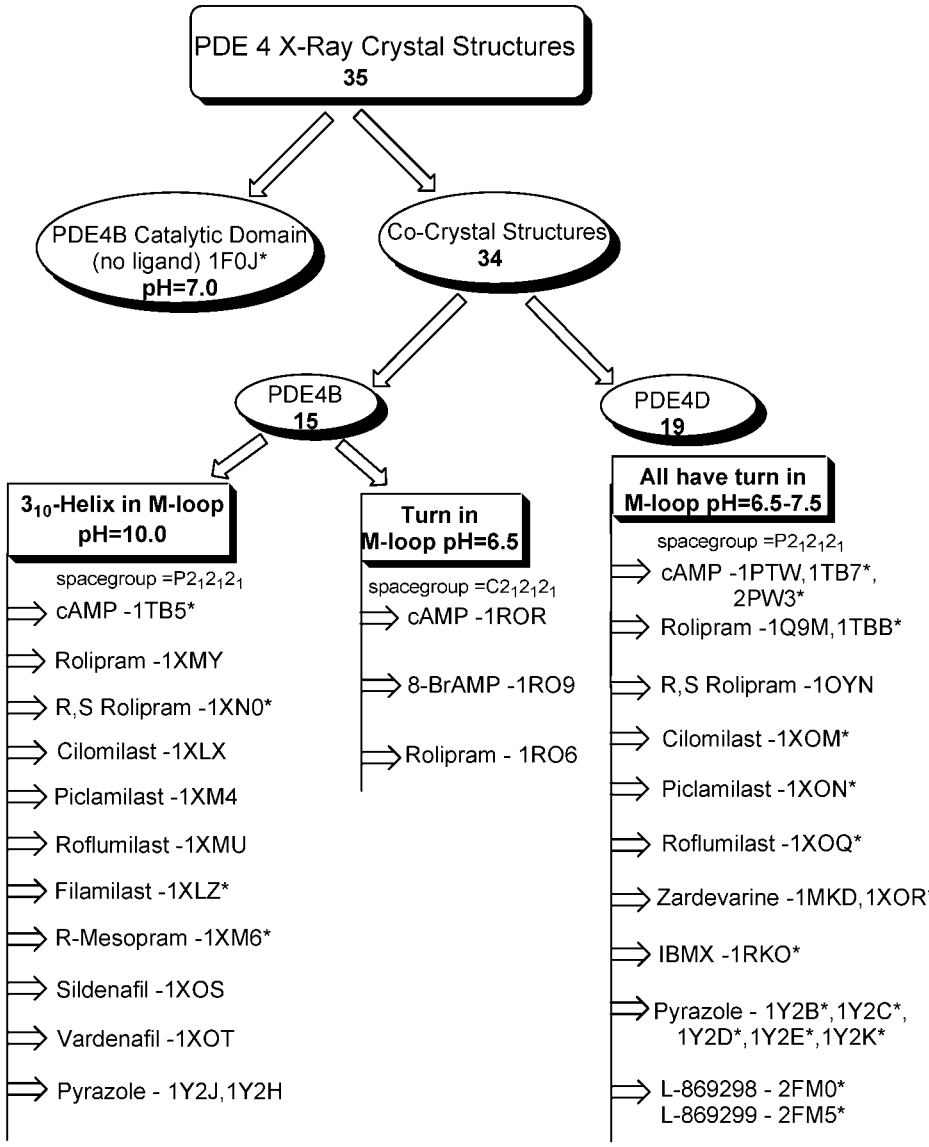

* pertains to those PDB structures that have water or solvent molecules near to the M-loop region.

Figure 1. Details of the available X-ray crystallographic structures of PDE4 with various ligands deposited in the Protein Data Bank.

tion with inhibitors such as rolipram analogs[6a,8b] and exists in various conformations with the NVP inhibitor.[11] Is this structural change a determining factor for the subtype selectivity? We identify that an experimental variable pH seems to be controlling this structural variation rather than the sequential differences in the PDE4. The influence of pH is studied by calculating the various protonation states of side chains or amide bonds of these structures in the gas and explicit solvent phases. An electronic structure explanation is given for this observation.

Computational Details

Root Mean Square Deviation (rmsd). Residue-by-residue rmsd is calculated using a FORTRAN program.[14] RMSDs are calculated for the backbone residues of all 4B and 4D crystal structures having similar ligands. A molecular operating environment (MOE) homology module[15] is used for structural alignment of 4B and 4D structures. The rmsd values are calculated using the following equation where d_i is the distance between the ith atoms and n is the number of such distances.

$$\mathrm{RMSD} = \sqrt{\sum_{i}^{n} d_i^2 / n}$$

Electronic Structure Calculation. We have used ab initio calculations on the model structures, generated from the fragment SPMCD (Ser, Pro, Met, Cys, Asp) residue sequence of PDE4B and PDE4D PDB coordinates. The resulting dangling valencies are saturated by appropriately placing hydrogens. For uniformity and to average out the specific differences in the geometries arising from the process of formation of the crystals, only the hydrogen atom positions in each of the structures are optimized. The dihedral angles are kept constant during this process. The protonated and

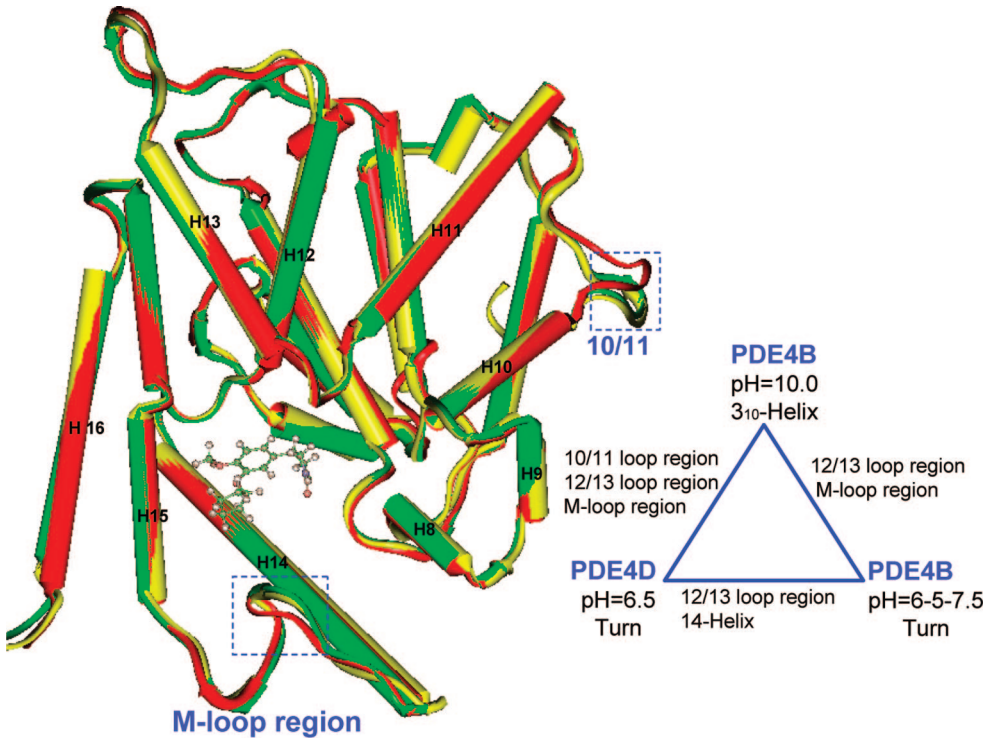

Figure 2. The superimposition of the α-carbon of the turn having PDE4B and PDE4D and a 3_{10}-helix having PDE4B structures with rolipram are shown with the yellow, green, and red color secondary structure at pH = 6.5, 7.0, and 10.0, respectively (left side). The ball and stick model represents the rolipram ligand in the active site. A schematic representation of structural differences with all the other similar ligands is also shown (right side).

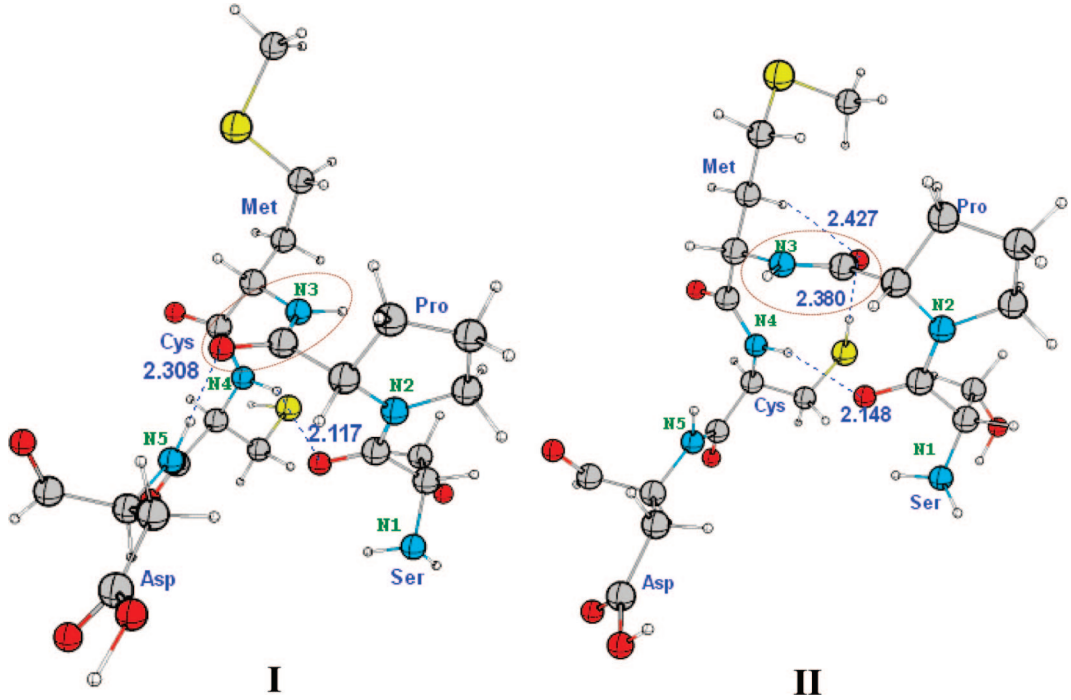

Figure 3. The optimized conformations, **I** (3_{10}-helix) and **II** (turn), of SPMCD residues at pH = 10.0 and pH = 6.5−7.5, respectively.

deprotonated states of aspartic acid and cysteine and amide bonds are calculated for seven sets of ligands. All electronic structure calculations are performed at the B3LYP/6−31+G* level of theory.[16]

The gas phase optimized model structures 1TB5 having a 3_{10}-helix and 1TB7 having a turn are further taken, and a layer of 5 Å thickness of water molecules is added using the "soak" option in InsightII.[17] The total number of water molecules present around the pentapeptide−protein structure is 119. The water molecules of the proteins are generally treated as low layer with molecular mechanics in QM/MM calculations to reduce the computational cost. The ONIOM[18,19]

Table 1. Reaction Energies in kcal/mol for Eq 1

ligand	I	II	ΔH
cAMP	1TB5	1ROR	−4.00
	1TB5	1TB7	−8.75
rolipram	1XMY	1RO6	2.78
	1XMY	1TBB	−0.13
R,S-rolipram	1XN0	1OYN	−9.68
cilomilast	1XLX	1XOM	−10.78
roflumilast	1XMU	1XOQ	−14.30
piclamilast	1XM4	1XON	−9.82
pyrazole	1Y2J	1Y2K	−4.48

Table 2. Reaction Energies in kcal/mol for Eq 2

ligand	I	II	ΔH
cAMP	1TB5	1ROR	−20.80
	1TB5	1TB7	−10.87
rolipram	1XMY	1RO6	−39.32
	1XMY	1TBB	−24.68
R,S-rolipram	1XN0	1OYN	−23.36
cilomilast	1XLX	1XOM	−19.79
roflumilast	1XMU	1XOQ	−23.80
piclamilast	1XM4	1XON	−15.21
pyrazole	1Y2J	1Y2K	−16.72

calculation is implemented for this system to analyze the explicit solvent effect on the structures. A two layer ONIOM calculation is adopted for the system, where the pentapeptide sequence SPMCD is defined quantum mechanically (high layer) with the B3LYP/6−31+G* level of theory and the water molecules are defined as a low layer molecular mechanics part with a universal force field.[20] The ONIOM energy of the system is given as

$$E^{\mathrm{ONIOM(QM:MM)}} = E^{\mathrm{QM}}_{\mathrm{model}} + E^{\mathrm{MM}}_{\mathrm{real}} - E^{\mathrm{MM}}_{\mathrm{model}} = E^{\mathrm{high}}_{\mathrm{model}} + E^{\mathrm{low}}_{\mathrm{real}} - E^{\mathrm{low}}_{\mathrm{model}}$$

These calculations are done using the Gaussian03 program package.[21]

Molecular Dynamics Simulations. The simulations are performed using the PMEMD module of AMBER9 version[22] in the IBM BLUEGENE/L machine. The deposited PDB structures 1TB5 and 1TB7 are taken for the molecular simulations. The coordinates of the M-loop region (423−440) of these protein structures are taken. The FF03 force field[23] is employed. The LEAP module is employed to construct a truncated octahedron solvate box (bcc) of cell length 56.46 Å with TIP3P water molecules around the protein. The solvation shell around the protein is 12 Å. The total number of solute and solvent atoms present around the 1TB5 and 1TB7 are 12578 and 12932, respectively. The protein−solvent system is minimized with 1000 steps of steepest descent and 2000 steps of conjugate gradient method. The protein is fixed during minimization using a harmonic constraint with a force constant of 500 kcal/mol/Å^2. This is done to remove any close contacts existing in the water shell with respect to protein. The whole system is also minimized after this for 200 steps steepest descent and 800 steps conjugate gradient method, so that the hydrogens of protein are optimized. The minimized structure obtained is then gradually heated up (over 40 ps) from 0 K to 300 K with harmonic constraints on solute using the SHAKE method. The dynamics is maintained under constant pressure-constant temperature (NPT) conditions using Berendsen (weak-coupling) temperature with a time step of 2 fs.[24] Finally, a production dynamics of 10 ns with protein is fixed under NPT conditions with a time step of 1 fs. The long-range interactions are calculated by the particle mesh Ewald (PME) method.[25] The grid size of 60 × 60 × 60 with grid spacing of 1.0 Å with a direct sum tolerance of 0.00001 and 9.0 Å cutoff is used. The cubic B-spline of fourth order is interpolated in PME. The resulting trajectories of molecular simulations are analyzed using the PTRAJ module of AMBER 8.0.

Results and Discussion

(a) Crystal Structure Analysis. There are about 60 PDE crystal structures in the PDB and 35 of these belong to the PDE4 class with various substrates such as cyclic adenosine monophosphate (cAMP), AMP, and 8-BrAMP and inhibitors such as rolipram analogs (rolipram, cilomilast, piclamilast, roflumilast, mesopram, and filamilast) and pyrazole analogs (Figure S1).[4−10] PDE4 is coded by four genes named as A, B, C, and D and are called subtypes. Among the four genes coding for PDE4, about 16 4B and 19 4D structures are crystallized (Figure 1). There is one each for PDE4 subtype with the NVP ({4-[8-(3-nitrophenyl)-[1,7]napthyridin-6-yl]benzoic acid}) inhibitor containing structures which are yet to be deposited.[11] The catalytic domain of the first crystal structure available for PDE4B contains 376 residues and explains the general architecture of PDE4.[4] The PDE4 has basically three subdomains comprising 17 α helices and a β hairpin. The catalytic pocket contains two divalent metal ions (Zn and Mg) that are crucial in hydrolysis of the substrate. Zn in the active site pocket has distorted trigonal bipyramid geometry, coordinating with Asp^{275}, Asp^{392}, His^{233}, His^{274}, and a water molecule of the protein.[13] On the other hand Asp^{275} of the protein and five water molecules surround the Mg atom. Furthermore the cocrystals of PDE4 with various ligands also have similar three subdomains comprising 16 α helices and a β hairpin (Figure 2).[5−10] Other than the conservation of helices and hairpin we noticed a surprising characteristic feature in these 35 structures: 12 structures have a 3_{10}-helix in the M-loop region. The remaining 23 of them have a turn in the M-loop region,[6b] 19 of these 23 belong to the PDE4D, and 4 belong to PDE4B (Figure 1).

(b) Root Mean Square Deviation (rmsd). We superimposed all structures having the 3_{10}- helix and the turn with seven similar sets of ligands, and the rmsd of residue by residue for the backbone is calculated.[14] There are two structures each for 4B and 4D with cAMP, three each with rolipram, and one each with cilomilast, piclamilast, roflumilast, and pyrazole analogs (Figure 1). The superimposition of 4B containing a 3_{10}-helix and 4D with similar ligand structures showed a major difference in three loop regions i.e., 10/11, 12/13, and the M-loop region (Figure 2). The residues with varying rmsd are Glu^{317} and Glu^{318} of helix 10/11 (316−319) which interacts with upstream conserved region (UCR)[1] UCR1 and UCR2 present in the regulatory domain (N-terminal) of the protein. The residues Ser^{368} and Ser^{369} of helix 12/13 (367−377) belonging to an extracellular signal-regulated kinases (ERK) docking site[1] that has

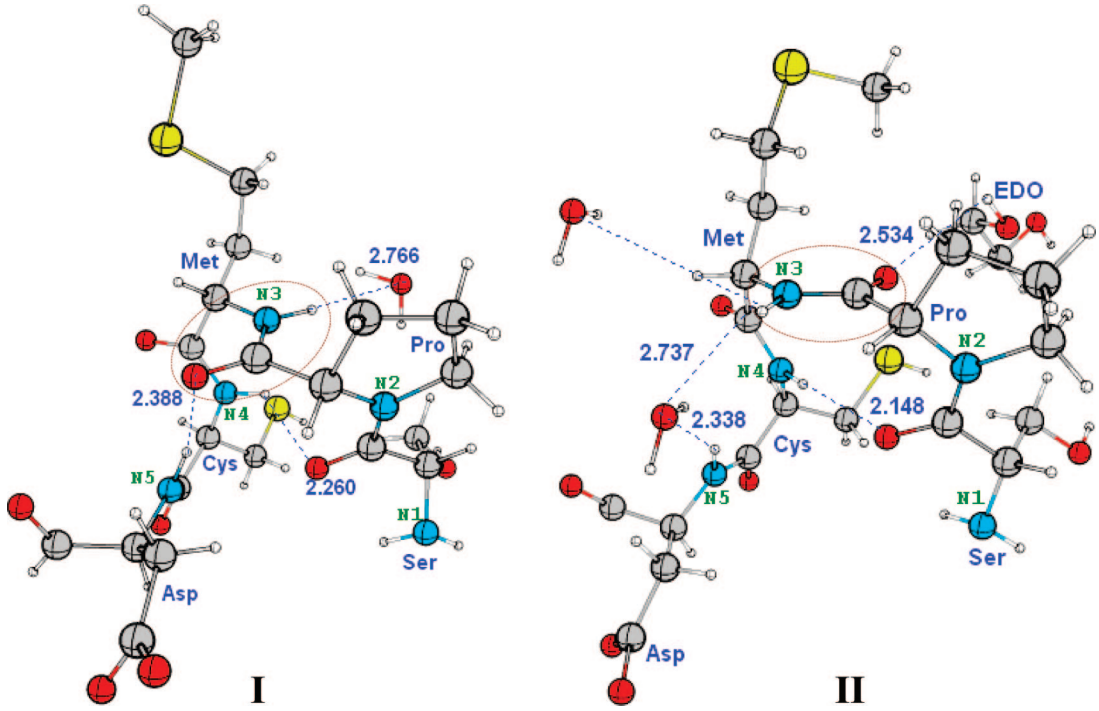

Figure 4. The X-ray crystal structural conformations of **I** (3_{10}-helix 1TB5) and **II** (turn 1TB7) at pH = 10.0 and pH = 6.5−7.5, respectively. In the SPMCD residue sequence the hydrogen bonding interaction of the amide bond with solvent molecules such as water and EDO is also shown.

protein−protein interactions is also altered. In the case of the M-loop region[6b] (424−437) Pro^{430} and Met^{431} residues are altered in the backbone of protein structure (Figures S2−S4). The extent of deviation in the ERK docking site varies slightly with the ligands.

On the other hand the superimposition of the 4B and 4D structures containing a turn with cAMP and rolipram shows a difference only in the 12/13 loop region (ERK docking site) and in helix 14, particularly from the residues Lys^{422} to Glu^{427} that are oriented toward the solvent region (Figures S2 and S3). The superimposition of all the 4B with cAMP and rolipram structures has a difference in 10/11 and the M-loop region (Figure 2). In spite of the major homology sequence similarity between 4B and 4D subtypes the common differences are found in the 12/13-loop region and either at the starting of the M-loop region or at the Pro^{430} residue. Thus the PDE4 structures can be divided into the two groups: one with the 3_{10}-helix and the other with the turn varying at 10/11 and in the M-loop region (Figure 2).

(c) Importance of Secondary Structural Change and Its Cause. In view of the important role of the secondary structural alterations in specific enzymatic functions of PDE5,[26] the M-loop region in PDE4 is scrutinized because the methionine residue here has hydrophobic interactions with all rolipram analogs.[6a,8b] The inhibitor selectivity of rolipram analogs to PDE4 is due to the hydrophobic interactions at the Q2 pocket, where methionine of the M-loop region is a constituent. The PDE 4A, 4B, 4C, and 4D with NVP, a subtype selective inhibitor also have shown large conformational changes of methionine having relatively high B-factors.[11] The conformational changes of methionine thus can have an impact on inhibitor binding. The analysis of these variations in PDE4 may help to understand the influence of the M-loop region in inhibitor selectivity.

The secondary structural difference of PDE4 crystals cannot be explained by the ligand binding or crystal packing or mutated residues. This is because there is a structural variation of a 3_{10}-helix and a turn in the M-loop region within PDE4B structures with the similar ligands and the same space group (Figure 1). The SPMCD residue sequence is conserved in all subtypes and hence cannot account for this structural difference. After an extensive search, the only difference we could find between these two sets of structures is the pH maintained during crystallization. Without any exception it was found that all the PDE4B structures having a 3_{10}-helix are crystallized at pH=10.0 from the polar solvents such as aqueous $LiSO_4$ and NH_4SO_4 solution. In contrast, all the turn containing 4B and 4D structures are obtained at the pH = 6.5−7.5 range with polyethylene glycol (PEG) conditions (Figure 1). Though we do not know the reason for the use of different pHs in these experiments, the results are surprising because in these examples the pH appears to dominate over the differences in sequences of PDE4B and 4D.

(d) Influence of pH on the M-Loop Region. As a first approximation we assume that the pH dependence on the different conformations is caused by the loss or gain of a proton that leads to ionizations of carboxylates and amines.[27] The changes in the electrostatic environment of PDE4B and 4D may alter the conformations and finally affect the secondary structure of the protein. The influence of the pH on the structure is known for lysozymes, plastocyanin, γ-chymotrypsin, azurin, and insulin.[28] Another example is of cubic insulin crystals that manifest alterations in the

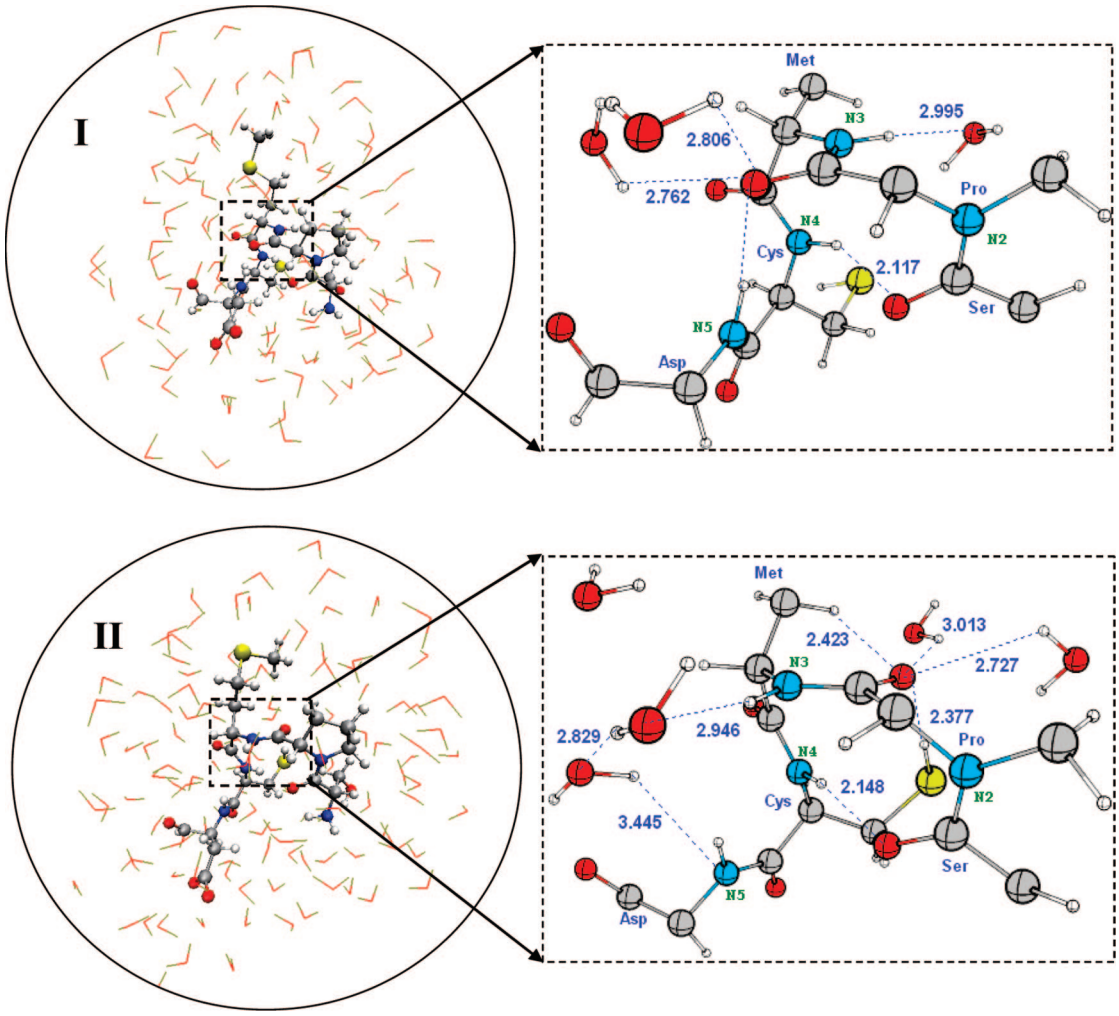

Figure 5. The ball and stick model represents the pentapeptide (SPMCD) that is considered the high layer QM region, and the shell with water molecules (lines) is considered as the low layer MM region. The optimized geometry of **I** and **II** and their hydrogen bonding network with the solvent−water molecules are also shown.

Table 3. Summary of a Number of Water Molecules Present Around PDE4B (1TB5) and PDE4D (1TB7) Structures

	no. of water molecules near to CO group of proline			no. of water molecules near to NH group of methionine		
structure	crystal	ONIOM	MD(10 ns)	crystal	ONIOM	MD(10 ns)
1TB5 (PDE4B)	0	2	1−2	1	2	0−2
1TB7 (PDE4D)	1 EDO	2	1−2	2	2−3	2−4

conformations of side chains of acidic residues as a function of the pH ranging from 7 to 11.[28] Such an alteration in the protonation states of acidic residues influencing the enzymatic role is well-known for the cytochrome P-450s.[29] The difference in the conformation around the 10/11 loop region of PDE4 as a function of the pH might arise from the repulsion between the side chains of two glutamic acid residues that are adjacent to each other.

In the M-loop region the difference in the secondary structure is observed at the backbone of the SPMCD residue sequence that has conformation **I** in the 3_{10}-helix of PDE4B and **II** in all the turn containing PDE4B and 4D structures (Figure 3). Structures **I** and **II** have a conserved hydrogen bond between the CO of serine and the NH of cysteine. These two structures have a difference in the orientation of the carbonyl group of the proline in the amide bond. This difference of the carboxy group orientation of the proline helps to gain extra hydrogen bonding with the NH group of the aspartic acid resulting in a twist and forming a 3_{10}-helix structure in **I** (Figure 3, Scheme 1C). Generally the constrained geometry of the proline initiates the turning of a protein strand, while here it brings a 3_{10}-helix structure of the conformation I.

The influence of pH can lead to the existence of various protonation states of side chains or amide bonds in structures **I** and **II**. The aspartic acid and cysteine side chains are generally known to be protonated in various protein structures.[28−30] There are some examples of backbone amide bonds that undergo protonation when they are involved in interactions with a metal as in belomycin.[29c] So, we anticipate that in the SPMCD residue sequence depending on pH, aspartic acid or cysteine side chains or amide bonds can be

protonated. We simulate different pH conditions by adding or removing a proton of side chains or amide bonds. The energies of the protonated and deprotonated states of aspartic acid, cysteine and amide bonds in all seven sets of similar ligands having a "3_{10}-helix" and a "turn" containing structures are calculated. The protonation and deprotonation states of aspartic acid residue do not explain the existing structural variations (S1). The isodesmic equation 1 shows the energetics of the protonation and the deprotonation of the cysteine residue. Except in rolipram ligand containing structures, the formation of the protonation state of cysteine in structure **II** and the deprotonated state in structure **I** are exothermic in the gas phase (Table 1).

$$\mathrm{I} + \mathrm{II}_{\mathrm{deprocys}} \rightarrow \mathrm{I}_{\mathrm{deprocys}} + \mathrm{II} \qquad (1)$$

The exothermicity of the reaction is due to the cysteine side chain (SH) in the protonated state gaining a weak hydrogen bond with the CO group of the proline in structure **II**, whereas in the deprotonated state it is missing (Figure 3). On the other hand in structure **I,** the deprotonated state of the cysteine side chain can have weak electrostatic interactions with the NH group of methionine.[31] The protonated state of the cysteine side chain in **II** and the deprotonated state in **I** have gained a noncovalent interaction each justifying their thermodynamic stabilities.

The feasibility of protonation of backbone amide bonds is also studied. Even though the differences of pH by three units may not lead to the protonation and deprotonation of amide bonds of PDE4 under experimental conditions, we anticipate that the protonation and deprotonation of N2 and N3 (Figure 3) of structures **I** and **II** would be an indicator of the influence of the pH. The deprotonation and protonation are done at N3 (NH of methionine) and N2 (N of proline) of the amide bonds, respectively, where the change of conformation is observed (Figure 3). Reaction energies of the isodesmic eq 2 for seven sets of similar ligands in their protonated and deprotonated states indicate that **II** is more stable in the protonated form and **I** in the deprotonated form (Table 2). The isodesmic eq 5 shows that all turn containing PDE4 (**II**) on protonation at N2 are stable over 3_{10}-helix containing structures (**I**), and in isodesmic eq 6 the reverse is observed for deprotonation at N3 (Tables S2 and S3).

The order of stability of the protonated state in all **II** and deprotonated form in **I** is attributed to the increase in the number of hydrogen bonding interactions. In structure **II,** the CO of the proline gains a 1,4 interaction with N2 on protonation and a weak interaction with the CH and SH of methionine and cysteine side chain residues.[31,32] On the other hand the deprotonation of N3 leads to a weak C−H−N3 interaction[33] in **I** similar to the C−H−O interaction seen in **II** (Figure 3). The thermodynamic stability of the protonated and the deprotonated states in structures **I** and **II** depends on the gain in noncovalent interactions such as hydrogen bonds and electrostatic interaction with the surrounding environment. The exothermicity of the backbone amide bond protonation is quite higher than cysteine protonation.

$$\mathbf{I}_{\mathrm{pro}} + \mathbf{II}_{\mathrm{depro}} \rightarrow \mathbf{I}_{\mathrm{depro}} + \mathbf{II}_{\mathrm{pro}} \qquad (2)$$

The extent of noncovalent interactions in structures **I** and **II** can also differ with respect to the surrounding solvent molecules. The 35 crystal structures are thus thoroughly examined near the M-loop region to know the influence of the water molecules. In all the crystal structures with respect to the methionine of the M-loop region a sphere radius of 10.0 Å is analyzed. There are 22 turn containing structures crystallized in PEG conditions. We found that the turn containing (**II**) PDE4D structures with resolution lower than 2.10 Å have ethane diol (EDO) and water molecules in this region (Table S4). The carbonyl group of the proline of structure **II** has a hydrogen bonding interaction with the EDO or water molecule. The amide group of the methionine of structure **II** has a hydrogen bonding network with the NH of aspartic acid through two water molecules (Figures 4 and S5). These additional interactions with the solvent thus stabilize structure **II**. The presence of EDO near the carbonyl group of proline in these structures may be due to PEG crystallization conditions, while such a type of EDO or water molecules are not found at the carbonyl group of proline in the M-loop region of four PDE4B (1F0J, 1ROR, 1RO6, and 1RO9) and in high resolution PDE4D turn containing structures, even though they have similar crystallization conditions (Table S4). Even the number of water molecules varies from 1−2 in the two chains (A and B) of the same crystal. This is also true in other crystals considered here (Table S4). It is possible to identify a water molecule even in the 12 low resolution structures with a 3_{10}-helix showing hydrogen bonding interaction to the amide group of methionine and carbonyl group of proline (Figures 4 and S5). The number of solvent molecules present around the M-loop region in these crystal structures is varied (Table S4).

The irregularity in the number and position of the water and the EDO molecules in the crystal structures led us to study the influence of the solvent molecules on the structures. We model this by constructing a layer of 5 Å thickness of water molecules around the pentapeptide SPMCD residue sequence of structures **I** and **II**. This model system with various protonation states of the cysteine and the amide bonds of 1TB5 and 1TB7 are studied using the QM/MM ONIOM method. In this model the pentapeptide is defined as the QM region and water molecules in the MM region (Figure 5). The ONIOM energies of the protonated and the deprotonated states of the cysteine and the amide bond (N2 and N3) in structures **I** and **II** along with a water layer are given in isodesmic eqs 3 and 4, respectively.

$$\mathbf{I} + \mathbf{II}_{\mathrm{deprocys}} \rightarrow \mathbf{I}_{\mathrm{depro\ cys}} + \mathbf{II} \quad \Delta \mathrm{E}^{\mathrm{ONIOM}} = -6.55\ \mathrm{kcal/mol} \qquad (3)$$

$$\mathbf{I}_{\mathrm{pro}} + \mathbf{II}_{\mathrm{depro}} \rightarrow \mathbf{I}_{\mathrm{depro}} + \mathbf{II}_{\mathrm{pro}} \quad \Delta E^{\mathrm{ONIOM}} = -10.06\ \mathrm{kcal/mol}$$
$$(\text{where } \mathbf{I} = 1\mathrm{TB5} \text{ and } \mathbf{II} = 1\mathrm{TB7}) \qquad (4)$$

The ONIOM calculation in explicit solvent shows the reaction is exothermic and similar as in the gas phase reaction (isodesmic eqs 1 and 2). The water molecules form a hydrogen bond with the NH group of methionine and the CO group of proline in structures **I** and **II**. The gain in the hydrogen bonding interaction of the amide bond in structure **II** makes it more stable than **I**. The hydrogen bonding

network of water with the residues in the crystal structures is reproduced by ONIOM calculations (Figures 4, S5, and 5).

To reinvestigate the average number of water molecules that can exist near the amide bond, the CO group of the proline, and the NH group of the methionine, MD simulation on M-loop region of a 3_{10}-helix (1TB5) and a turn (1TB7) containing structures are performed for 10 ns in explicit solvent under NPT conditions. The simulation result also shows similar hydrogen bonding interactions of water molecules around the CO group of the proline and the NH group of the methionine. The number of water molecules present around the NH group of the methionine and the CO group of the proline are retained as in ONIOM model systems (Figures S6 and S7 and Table 3). The gas phase, ONIOM, and MD calculations of the model systems have shown noncovalent interactions with adjacent residues, and solvent molecules in structures **I** and **II** are different.

Electronic structure calculations thus explain the structural anomaly that at pH = 10.0 conformation **I** is seen in all 3_{10}-helix PDE4B structures and at pH = 6.5−7.5 prefer conformation **II** as observed in all turn containing crystal structures. The pH variation thus can have different protonation states of cysteine side chain or backbone amide bonds. The different protonated states are stabilized by the noncovalent interactions of the amide bond with the surrounding environment such as adjacent residues and solvent molecules. Thus the orientation of the amide bond between proline and methionine is the deciding factor for the secondary structural change in the **II** or **I**. The pH dependence of the structures shows that there will be potential differences in the interaction at different parts of the cells in the body at different pH for the same enzyme−substrate combination. The secondary structure difference presented here has similar sequences and cannot account for subtype selectivity of PDE4 because at physiological pH it could have a turn structure. However, the variation in the sequence of the M-loop region may change the interactions with the inhibitor that can help in subtype selectivity. The exploration of the PDE4 inhibitor that can accommodate the M-loop region apart from the metal[8b,9] and the solvent pocket[34] of the active site can lead to better subtype selectivity.

Conclusions

The 35 X-ray crystal structures of the two subtypes of PDE4 show an influence of pH of the crystallization medium as an experimental variable on the secondary structural change in the M-loop region. The pattern of secondary structural change in the highly flexible M-loop region as a function of pH is striking in these crystal structures. Electronic structure calculations on the model sequence of the SPMCD residue of PDE4 explain the thermodynamic preferences for the secondary structure in the pattern of a 3_{10}-helix versus a turn in the M-loop region. The protonated states of the cysteine side chain and amide bond of turn containing structures are exothermic according to the isodesmic equations. It is due to the increase in the number of hydrogen bonding interactions with a surrounding environment such as adjacent residues and solvent molecules. Thus the variations in local (physiological) pH at the point of interaction can be an added parameter in optimizing the specificity of PDE4 inhibitors.

Acknowledgment. We thank CMSD and HPCF of the University of Hyderabad, MHPCC at Hawaii, and SERC of IISc for computing facilities. We thank Prabal Maiti for helping in the installation of AMBER 9.0 on a BLUE GENE/L machine. We thank DBT and DST for financial assistance. D.U.R. and P.S. also thank CSIR for fellowships.

Supporting Information Available: Structures of ligand in the cocrystals of various PDBs and the root-mean-square deviation graphs with various structures, isodesmic equations, total energies and Cartesian coordinates for optimized geometries, and graphs of water shell around the amide group of 1TB5 and 1TB7 in a 10 ns MD simulation. This material is available free of charge via the Internet at http://pubs.acs.org.

References

(1) (a) Bender, A. T.; Baevo, A. J. Cyclic Nucleotide Phosphodiesterases: Molecular Regulation to Clinical Use. *Pharmacol Rev.* **2006**, *58*, 488–520. (b) Houslay, M. D. PDE4-cAMP-specific Phosphodiesterases. *Prog. Nucleic Acid Res. Mol. Biol.* **2001**, *69*, 249–315. (c) Chung, K. F. Phosphodiesterase Inhibitors in Airways Disease. *Eur. J. Pharmacol.* **2006**, *533*, 110–117. (d) Boswell-Smith, B.; Spina, D.; Page, C. P. Phosphodiesterase inhibitors. *Br. J. Pharmacol.* **2006**, *147*, S252−S257.

(2) (a) Castro, A.; Jerez, M. J.; Martinez, A.; Gil, C. Cyclic nucleotide Phosphodiesterases and their Role in Immunomodulatory Responses: Advances in the Development of Specific Phosphodiesterase Inhibitors. *Med. Res. Rev.* **2005**, *25*, 229–244. (b) Zhang, K. Y. J.; Ibrahim, P. N.; Gillette, S.; Bollag, G. Phosphodiesterase 4 as a Potential Drug Target. *Exp. Opin. Ther. Drugs* **2005**, *9*, 1283–1304. (c) Houslay, M. D.; Schafer, P.; Zhang, K. Y. J. Phosphodiesterase-4 as Therauptic target. *Drug Discovery Today* **2005**, *10*, 1503–1519.

(3) (a) Jeon, J. H.; Heo, Y.-S.; Kim, C. M.; Hyun, Y.-L.; Lee, T. G.; Ro, S.; Cho, J. M. Phosphodiestrase: Overview of Protein Structures, Potential Therapeutic Applications and Recent progress in Drug Development. *Cell. Mol. Life Sci.* **2005**, *62*, 1198–1220. (b) Srivani, P.; Srinivas, E.; Raghu, R.; Sastry, G. N. Molecular Docking Studies of Pyridopurinone Derivatives - Potential Phosphodiesterase5 Inhibitor. *J. Mol. Graphics Modell.* **2007**, *26*, 378–390.

(4) Xu, R. X.; Hassell, A. M.; Vanderwall, D.; Lambert, M. H.; Holmes, W. D.; Luthe, M. A.; Rocque, W. J.; Milburn, M. V.; Zhao, Y.; Ke, H.; Nolte, R. T. Atomic structure of PDE4: Insight into Phosphodiesterase Mechanism and Specificity. *Science* **2000**, *288*, 1822–1825.

(5) Lee, M. E.; Markowitz, J.; Lee, J.-O.; Lee, H. Crystal structure of Phosphodiesterase 4D and Inhibitor complex. *FEBS Lett.* **2002**, *530*, 53–58.

(6) (a) Huai, Q.; Wang, H.; Sun, Y.; Kim, H.-Y.; Liu, Y.; Ke, H. Three-dimensional Structures of PDE4D in Complex with Roliprams and Implication on Inhibitor selectivity. *Structure* **2003**, *11*, 865–873. (b) Huai, Q.; Liu, Y.; Francis, S. H.; Corbin, J. D.; Ke, H. Crystal structures of Phosphodiesterases 4 and 5 in Complex with Inhibitor 3-isobutyl-1-Methyl Xanthine suggest a Conformation Determinant of Inhibitor Selectivity. *J. Biol. Chem.* **2004**, *279*, 13095–13101.

(7) (a) Huai, Q.; Colicelli, J.; Ke, H. The crystal structure of AMP-bound PDE4 Suggests a Mechanism for Phosphodiesterase Catalysis. *Biochemistry* **2003**, *42*, 13220–13226. (b) Xu, R. X.; Rocque, W. J.; Lambert, M. H.; Vanderwall, D. E.; Luther, M. A.; Nolte, R. T. Crystal structures of the Catalytic Domain of Phosphodiesterase 4B complexed with AMP, 8-Br-AMP, and Rolipram. *J. Mol. Biol.* **2004**, *337*, 355–365.

(8) (a) Zhang, K. Y. J.; Card, G. L.; Suzuki, Y.; Artis, D. R.; Fong, D.; Gillette, S.; Hsieh, D.; Neiman, J.; West, B. L.; Zhang, C.; Milburn, M. V.; Kim, S.-H.; Schlessinger, J.; Bollag, G. A. Glutamine Switch Mechanism for Nucleotide Selectivity by Phosphodiesterases. *Mol. Cell* **2004**, *15*, 279–286. (b) Card, G. L.; England, B. P.; Suzuki, Y.; Fong, D.; Powell, B.; Lee, B.; Luu, C.; Tabrizizad, M.; Gillette, S.; Ibrahim, P. N.; Artis, D. R.; Bollag, G.; Milburn, M. V.; Kim, S.-H.; Schlessinger, J.; Zhang, K. Y. J. Structural Basis for the Activity of Drugs that Inhibit Phosphodiesterases. *Structure* **2004**, *12*, 2233–2247.

(9) Card, G. L.; Blasdel, L.; England, B. P.; Zhang, C.; Suzuki, Y.; Gillette, S.; Fong, D.; Ibrahim, P. N.; Artis, D. R.; Bollag, G.; Milburn, M. V.; Kim, S.-H.; Schlessinger, J.; Zhang, K. Y. J. A Family of Phosphodiesterase Inhibitors Discovered by Cocrystallography and Scaffold-based drug design. *Nat. Biotechnol.* **2005**, *23*, 201–207.

(10) Huai, Q.; Sun, Y.; Wang, H.; Macdonald, D.; Aspiotis, R.; Robinson, H.; Huang, Z.; Ke, H. Enantiomer discrimination Illustrated by the High Resolution Crystal Structures of Type 4 Phosphodiesterase. *J. Med. Chem.* **2006**, *49*, 1867–1873.

(11) Wang, H.; Peng, M.; Chen, Y.; Geng, J.; Robinson, H.; Houslay, M. D.; Cai, J.; Ke, H. Structures of the Four subfamilies of Phosphodiesterase−4 provide Insight into the Selectivity of their Inhibitors. *Biochem. J.* **2007**, *408*, 193–201.

(12) Nelson, D. L.; Cox, M. M. *Amino acids, peptides and proteins. Lehninger Principles of Biochemistry,* 4th ed.; W. H. Freman and Company: 41 Madison Avenue, New York, 2006.

(13) (a) Millhauser, G. L. Views of Helical Peptides: A Proposal for the Position of 3_{10}-Helix along the Thermodynamic Folding Pathway. *Biochemistry* **1995**, *34*, 3873–77. (b) Wu, Y.-D.; Zhao, Y.-L. A Theoretical Study on the Origin of Cooperativity in the Formation of 3_{10}- and α-Helices. *J. Am. Chem. Soc.* **2001**, *123*, 5313–19. (c) Chin, W.; Piuzzi, F.; Dognon, J.-P.; Dimicoli, I.; Tardivel, B.; Mons, M. Gas Phase Formation of a 3_{10}-Helix in a Three-Residue Peptide Chain: Role of Side Chain-Backbone Interactions as Evidenced by IR-UV Double Resonance Experiments. *J. Am. Chem. Soc.* **2005**, *127*, 11900–01.

(14) Bindu, P. H.; Sastry, G. M.; Murty, U. S. N.; Sastry, G. N. Structural and Conformational Changes Concomitant with the E1-E2 Transition in H+K+-ATPase: A Comparative Protein Modeling Study. *Biochem. Biophys. Res. Commun.* **2004**, *319*, 312–320.

(15) MOE version 2006; Chemical Computing Group, 954, First Floor, 16th Main, BTM Layout 2nd Stage, Bangalore, India 560 076.

(16) (a) Becke, A. D. Density-functional Thermochemistry. III. The role of exact exchange. *J. Chem. Phys.* **1993**, *98*, 5648–5652. (b) Becke, A. D. Density-Functional Exchange-Energy Approximation with Correct Asymptotic Behavior. *Phys. Rev. A* **1988**, *38*, 3098–3100.

(17) Insight II Version 2000; Molecular Modelling System 2000 Molecular Simulations: 9685 Scrantan Road, San Deigo, CA.

(18) Dapprich, S.; Komáromi, I.; Suzie Byun, K.; Morokuma, K.; Frisch, M. J. A new ONIOM implementation in Gaussian98. Part I. The Calculation of Energies, Gradients, Vibrational Frequencies and Electric Field Derivatives. *J. Mol. Struct. (Theochem)* **1999**, *462*, 1–21.

(19) Vreven, T.; Morokuma, K.; Farkas, Ö.; Schlegel, H. B.; Frisch, M. J. Geometry Optimization with QM/MM, ONIOM, and Other Combined Methods. I. Microiterations and Constraints. *J. Comput. Chem.* **2003**, *24*, 760–769.

(20) Rappé, A. K.; Casewit, C. J.; Colwell, K. S.; Goddard, W. A., III; Skiff, W. M. UFF, A Full Periodic Table Force Field for Molecular Mechanics and Molecular Dynamics Simulations. *J. Am. Chem. Soc.* **1992**, *114*, 10024–35.

(21) *Gaussian 03, Revision B.03*, Frisch, M. J.; Trucks, G. W.; Schlegel, H. B.; Scuseria, G. E.; Robb, M. A.; Cheeseman, J. R.; Montgomery, J. A., Jr.; Vreven, T.; Kudin, K. N.; Burant, J. C.; Millam, J. M.; Iyengar, S. S.; Tomasi, J.; Barone, V.; Mennucci, B.; Cossi, M.; Scalmani, G.; Rega, N.; Petersson, G. A.; Nakatsuji, H.; Hada, M.; Ehara, M.; Toyota, K.; Fukuda, R.; Hasegawa, J.; Ishida, M.; Nakajima, T.; Honda, Y.; Kitao,O.; Nakai, H.; Klene, M.; Li, X.; Knox, J. E.; Hratchian, H. P.; Cross, J. B.; Bakken, V.; Adamo, C.; Jaramillo, J.; Gomperts, R.; Stratmann, R. E.; Yazyev, O.; Austin, A. J.; Cammi, R.; Pomelli, C.; Ochterski, J. W.; Ayala, P. Y.; Morokuma, K.; Voth, G. A.; Salvador, P.; Dannenberg, J. J.; Zakrzewski, V. G.; Dapprich, S.; Daniels, A. D.; Strain, M. C.; Farkas, O.; Malick, D. K.; Rabuck, A. D.; Raghavachari, K.; Foresman, J. B.; Ortiz, J. V.; Cui, Q.; Baboul, A. G.; Clifford, S.; Cioslowski, J.; Stefanov, B. B.; Liu, G.; Liashenko, A.; Piskorz, P.; Komaromi,I.; Martin, R. L.; Fox, D. J.; Keith, T.; Al-Laham, M. A.; Peng, C. Y.; Nanayakkara, A.; Challacombe, M.; Gill, P. M. W. B.; Chen, W.; Wong, M. W.; Gonzalez, C.; Pople, J. A. Gaussian, Inc.: Wallingford, CT, 2003.

(22) Case, D. A.; Pearlman, D. A.; Caldwell, J. W.; Cheatham, T. E.; Wang, J.; Ross, W. S.; Simmerling, C.; Darden, T.; Merz, K. M.; Stanton, R. V.; et al. *AMBER9*, 9th ed.;University of California: San Francisco, CA.

(23) Duan, Y.; Wu, C.; Chowdhury, S.; Le, M. C.; Xiong, G.; Zhang, W.; Yang, R.; Cieplak, P.; Luo, R.; Lee, T.; Caldwell, J.; Wang, J.; Kollman, P. A Point-Charge Force Field for Molecular Mechanics Simulations of Proteins Based on Condensed-Phase Quantum Mechanical Calculations. *J. Comput. Chem.* **2003**, *24*, 1999–2012.

(24) Berendsen, H. J. C.; Postma, J. P. M.; van Gunsteren, W. F.; DiNola, A.; Haak, J. R. Molecular Dynamics with Coupling to An External Bath. *J. Chem. Phys.* **1984**, *81*, 3684–90.

(25) Darden, T.; York, D.; Pedersen, L. Particle mesh Ewald: An $N\cdot\log(N)$ Method For Ewald Sums in Large Systems. *J. Chem. Phys.* **1993**, *98*, 10089–92.

(26) Wang, H.; Liu, Y.; Huai, Q.; Cai, J.; Zoraghi, R.; Francis, S. H.; Corbin, J. D.; Robinson, H.; Xin, Z.; Lin, G.; Ke, H. Multiple Conformations Of Phosphodiesterase5 Implications For Enzyme Function and Drug Development. *J. Biol. Chem.* **2006**, *281*, 21469–21479.

(27) (a) Alexov, E. Numerical Calculations of the pH of Maximal Protein Stability. *Eur. J. Biochem.* **2004**, *271*, 173–185. (b) Schaefer, M.; Sommer, M.; Karplus, M. pH Dependence of Protein Stability: Absolute Electrostatic Free Energy Differences between Conformations. *J. Phys. Chem.* **1997**, *101*, 1663–1683. (c) Antosiewicz, J.; McCammon, J. A.; Gilson, M. K. Prediciton of pH-Dependent Properties of Proteins. *J. Mol. Biol.* **1994**, *238*, 415–436. (d) Pujato, M.; Navarro, A.; Versace, R.; Mancusso, R.; Ghose, R.; Tasayco, M. L. The

pH-dependence of Amide Chemical Shift of Asp/Glu Reflects its pk_a in Intrinsically Disordered Proteins with Local Interactions. *Biochim. Biophys. Acta* **2006**, *1764*, 1227–1233. (e) Thomas, P. G.; Russell, A. J.; Fersht, A. R. Tailoring the pH Dependence of Enzyme Catalysis using Protein Engineering. *Nature* **1985**, *318*, 375–376.

(28) Gursky, O.; Badger, J.; Li, Y.; Caspar, D. L. Conformational Changes in Cubic Insulin Crystals in the pH Range 7−11. *Biophys. J.* **1992**, *63*, 1210–1220.

(29) (a) Murthy, J. N.; Nagaraju, M.; Sastry, G. M.; Rao, A. R.; Sastry, G. N. Acitve site acidic residues and structural analysis of modeled human aromatase. *J. Comput.-Aided Mol. Des.* **2005**, *19*, 857–870. (b) Altun, A.; Guallar, V.; Friesner, R. A.; Shaik, S.; Thiel, W. The Effect of Heme Environment on the Hydrogen Abstraction Reaction of Camphor in $P450_{cam}$ Catalysis: A QM/MM Study. *J. Am. Chem. Soc.* **2006**, *128*, 3924–3925. (c) Kumar, D.; Hirao, H.; Shaik, S.; Kozlowski, P. M. Proton-Shuffle Mechanism of O-O Activation for Formation of a High-Valent Oxo-Iron Species of Bleomycin. *J. Am. Chem. Soc.* **2006**, *128*, 16148–16158.

(30) (a) Lide, D. R. *Handbook of Chemistry and Physics,* 84th ed.; CRC Press: Boca Raton, FL, 2003. (b) Thurlkill, R. L.; Grimsley, G. R.; Scholtz, J. M.; Pace, C. N. pK_a Values of The Ionizable Groups of Proteins. *Protein Sci.* **2006**, *15*, 1214–1218. (c) Dawson, R. M. C.; Elliot, D. C.; Elliot, W. H.; Jones, K. M. *Data for biochemical research,* 3rd ed.;Clarendon Press: Oxford, 1995. (d) Bombarda, E.; Morellet, N.; Cherradi, H.; Spiess, B.; Bouaziz, S.; Grell, E.; Roques, B. P.; Mély, Y. Determination of the pK_a of the four Zn^{2+}-Coordinating Residues Of The Distal Finger Motif of the HIV-1 Nucleocapsid Protein: Consequences on the Binding of Zn^{2+}. *J. Mol. Biol.* **2001**, *310*, 659–672. (e) Dudev, T.; Lim, C. Factors Governing The Protonation State of Cysteine In Proteins: An Ab initio/CDM study. *J. Am. Chem. Soc.* **2002**, *124*, 6759–66.

(31) Noar, M. M.; Jenson, J. H. Determinants of Cysteine pKa Values in Creatine Kinase and α-Antitrypsin. *Proteins: Struct., Funct., Bioinfor.* **2004**, *57*, 799–803.

(32) (a) Marino, T.; Russo, N.; Tocci, E.; Toscano, M. Density Functional Computations of Proton Affinity and Gas-Phase Basicity of Proline. *J. Mass. Spectrom.* **2001**, *36*, 301–305. (b) Sapse, A.-M. *Molecular orbital calculations for amino acids and peptides*; Birkhaüser, Boston, MA, 2000.

(33) Joseph, J.; Jemmis, E. D. Red-, Blue-, or No-Shift in Hydrogen Bonds: A Unified Explanation. *J. Am. Chem. Soc.* **2007**, *129*, 4620–4632.

(34) Krier, M.; de Araújo-Júnior, J. X.; Schmitt, M.; Duranton, J.; Justiano-Basaran, H.; Lugnier, C.; Bourguignon, J.-J.; Rognan, D. Design of Small-Sized Libraries by Combinatorial Assembly of Linkers and Functional Groups to a Given Scaffold: Application to the Structure-Based Optimization of a Phosphodiesterase 4 Inhibitor. *J. Med. Chem.* **2005**, *48*, 3816–3822.

CT700261B